Dry-Type Artificial Muscles Based on Pendent Sulfonated Chitosan and Functionalized Graphene Oxide for Greatly Enhanced Ionic Interactions and Mechanical Stiffness

Jin-Han Jeon, Ravi Kumar Cheedarala, Chang-Doo Kee, and Il-Kwon Oh**

Biopolymer-based artificial muscles are promising candidates for biomedical applications and smart electronic textiles due to their multifaceted advantages like natural abundance, eco-friendliness, cost-effectiveness, easy chemical modification and high electical reactivity. However, the biopolymer-based actuators are showing relatively low actuation performance compared with synthetic electroactive polymers because of inadequate mechanical stiffness, low ionic conductivity and ionic exchange capacity (IEC), and poor durability over long-term activation. This paper reports a high-performance electro-active nano-biopolymer based on pendent sulfonated chitosan (PSC) and functionalized graphene oxide (GO), exhibiting strong electro-chemo-mechanical interations with ionic liquid (IL) in open air environment. The proposed GO-PSC-IL nano-biopolymer membrane shows an icnreased tensile strength and ionic exchange capacity of up to 44.8% and 83.1%, respectively, and increased ionic conductivity of over 18 times, resulting in two times larger bending actuation than the pure chitosan actuator under electrical input signals. Eventually, the GO-PSC-IL actuators could show robust and high-performance actuation even at the very low applied voltages that are required in realistic applications.

1. Introduction

Recently, electroactive polymers (EAPs) have received great attention due to their attractive merits of biomimetic actuation, large deformation, quick response, relatively low-cost, thinness, flexibility, and light weight. Thus far, many different kinds of EAP materials, for example, polymer gel,[1] conducting polymers,[2,3] ionic polymer-metal composites (IPMC),[4–6] carbon nanotubes,[7,8] graphene nanosheets,[9–11] dielectric elastomers[12] and ferroelectric polymers[13] have been newly developed and deeply investigated. Electroactive polymers have been considered a challenging nature-inspired technology for various attractive applications such as soft organic electronics,[14] haptic devices,[15] biomimetic robots,[16] smart electronic textiles in biomedicine,[17] braille display,[18] bio-medical devices,[19] and biomimetic sensory-actuators.[20] Therefore, the development of high-fidelity electro-active polymers is crucial for successfully achieving those challenging applications.

Among EAPs, the IPMC actuator,[4] which has a sandwich structure composed of a core ionic polymer like Nafion or Flemion and noble metallic conductors such as platinum or gold, has several attractions including miniaturization, easy manufacturability, low power consumption and large bending deformation under low input voltage. Over two decades, several synthetic ionic polymers[21–25] have been developed to make high-performance IPMC actuators that are prerequisite for various industrial applications. However, some human-related applications such as smart electronic textiles and disposable biomedical devices will require biodegradable and biocompatible ionic exchangeable polymers. The best way to develop such an eco-friendly and biocompatible polymer actuator is to use naturally abundant biopolymers such as plant cellulose,[26] cellulose acetate,[27] and bacterial cellulose.[28] However, their actuation performances have not yet achieved the desirable target for practical applications.

As a biopolymer, chitosan has also attracted significant interest, because it has many active functional groups such as alcohols, amides and free amine groups with uniform natural nano to micro sized pores. Kim et al.[29] used chitosan layers to enhance the actuation performance of pure cellulose-based EAPap actuator. Recently, Chen et al.[30] developed a chitosan-based bimorph actuator with chitosan-wrapped MWCNT composites as conductive, mechanically robust and porous composite electroactive electrode layers. In addition, Xie et al.[31] reported fast-moving, high-power electromechanical actuators by using highly conductive single-walled carbon nanotube (SWNT) sheets. But previous studies were only focused on the

J.-H. Jeon, Dr. R. K. Cheedarala, Prof. I.-K. Oh
School of Mechanical
Aerospace and Systems Engineering
Korea Advanced Institute of Science and Technology
291 Daehak-ro, Yuseong-gu, Daejeon, 305-701,
Republic of Korea
E-mail: ikoh@kaist.ac.kr
Dr. R. K. Cheedarala, Prof. C.-D. Kee
School of Mechanical Systems Engineering
Chonnam National University
300 Yongbong-dong, Buk-gu, Gwang-Ju, 500-757, Republic of Korea;
E-mail: cdkee@chonnam.ac.kr

DOI: 10.1002/adfm.201203550

enhanced carbon electrode networks rather than the improvement of bare chitosan ionic biopolymer. Until now, the chitosan-based artificial muscles, which have relatively low mechanical stiffness and ionic conductivity compared wih synthetic ionic polymers, have not been improved with functionaliztion and reinforcement of chitosan biopolymer itself.

In order to develop a new type of low-cost, air working, eco-friendly electro-active biopolymer actuator with improved electro-chemo-mechanical properties, we report a simple route for a high-performance ionic conducting nano-biopolymer membrane based on pendent sulfonated chitosan and functionalized graphene oxide. The amine group in the chitosan biomolecule was actively used to tune the degre-of-sulfonation (DOS) of pendent sulfonated chitosan (PSC) by controlled treatment with 1,3-propyl sultone in ambient conditions and reacted with functionalized graphene oxide. Thus, it can act as a higher ionic-exchangable membrane because of the availability of propyl sulfonic acid groups that can strongly bind with free amines and with ionic liquid. Furthermore, electro-chemo-mechanical activities of PSC can be maximized by simply reinforcing with functionalized carbon nanomaterials.[25,32–34] Therefore, functionalized graphene oxide (GO) was used to improve in-plane mechanical stiffness and electro-chemo-mechanical properties through strong ionic interactions and bonding with free amines and sulfuric acid groups of PSC biopolymer. In detail, a protonation reaction can be activated in acid media and promote the strong ionic interactions between hydrophilic functional groups, i.e., -COOH and -OH of GO, and -SO_3H and -NH_2 of PSC. For air-working artificial muscles with wide potential window and high ionic conductivity, ionic liquid (IL), 1-ethyl-3-methylimidazolium trifluoromethane sulfonate (EMI.OTf), was used as liquid electrolytes within the polyelectrolyte matrix. EMI.OTf, which consists of cation(EMI^+)[35] and anion(OTf^-, $[CF_3SO_3]^-$)[36] as dissociated mobile ions under an electric field, binds loosely with sulfonated chistoan to support transport of ions in a dry environment. The schematic representation and chemical structures of the GO-PSC-IL ionic polymer membrane are shown in **Scheme 1**.

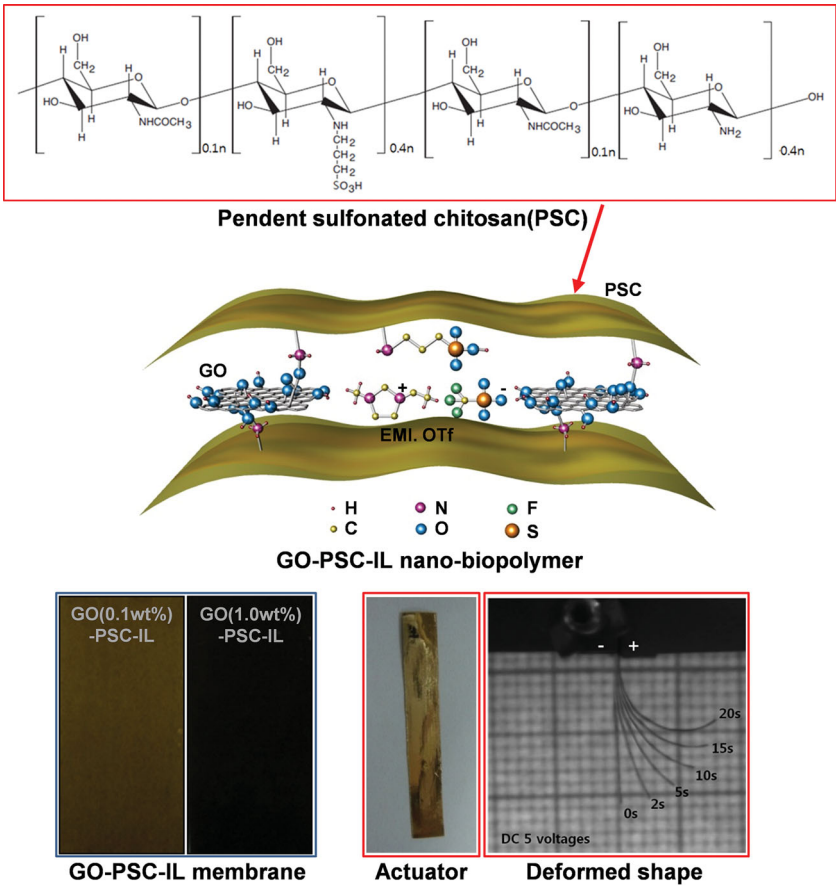

Scheme 1. Schematic illustration for pendent sulfonated chitosan and graphene oxide-pendent sulfonated chitosan-ionic liquid (GO-PSC-IL) nano-biopolymer actuator.

The average tensile strength of the GO(1.0 wt%)-PSC-IL actuator is ≈60 MPa, which is also moderately better than other chitosan-based actuators (50 MPa).[31] Surface and cross-sectional SEM images reveal the well dispersion of GO particles and the reduced pore size of GO-PSC-IL membranes. The crystallinity of membranes was confirmed by XRD pattern, and functional group interactions were determined using FT-IR spectroscopy. The incorporation of GO enhanced multiple qualities such as mechanical strength and physicochemical properties like ionic exchangeable capacity (IEC), ionic conductivity and electrochemical impedance, resulting in a novel high-performance nano-biopolymer actuator that shows very large bending deformations under low input voltages in a dry environment.

2. Results and Discussion

2.1. Synthesis of GO-PSC-IL Nano-Biopolymer Membrane

The chemical reaction of chitosan (degree of deacetylation, 80%) with 1,3-propane sultone to produce chitosan-N-propyl sulfonic acid is shown in **Figure 1**. Lien et al.[37] have reported various PSC membranes with different degrees of sulfonation (DOS), i.e., more than 60 DOS, to improve its hydrophilicity and water solubility. Due to the need of excessive free amine groups in chitosan for protonation reaction with graphene oxide and ionic liquid, and for moderate hydrophilicity, we have used 0.5 molar ratio of sulfonating agent, (i.e., 1,3-propane sultone) to glucosamine unit, where the number of 0.5 refers to the degree of substitution of alkyl sulfonic groups (DOS = 50%) in chitosan. Subsequently, the free amines in chitosan will be protonated with carboxylic acid groups of graphene oxide (GO) and sulfonic groups of PSC.

GO was prepared by oxidizing the pristine graphite using a modified Hummers method.[38] A high density of oxygen-containing functional groups, such as epoxide, carbonyl (C = O),

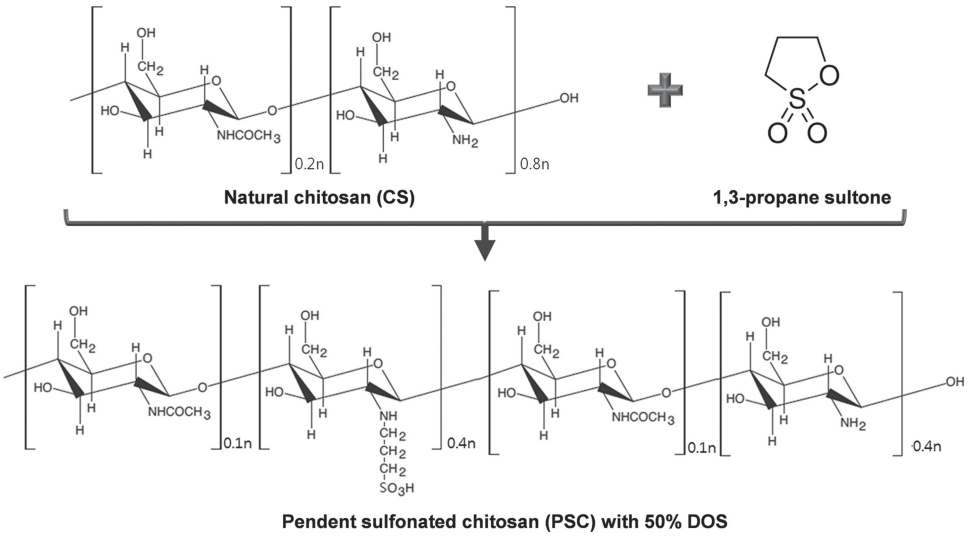

Figure 1. Synthesis of pendent sulfonated chitosan copolymer (PSC) with 50% DOS.

carboxyl (COOH), and hydroxyl (OH) groups attached to the GO surface typically cause GO sheets to be strongly hydrophilic and their aqueous dispersions to be stable. In addition, the above functionalities can show electrostatic repulsions between the GO sheets due to high densities of electro-negative groups as shown in Supporting Information Figure S1. X-ray diffraction patterns of the parent GO show the interlayer spacing, which indicates the complete transformation from graphite to GO as shown in Supporting Information Figure S2.

Well-dispersed GO-PSC nano-biopolymers were fabricated through a simple self-assembly and in-situ one-pot casting method by solution mixing as described in the Experimental Section. **Figure 2** shows the ionic interactions occurring on the blending pendent sulfonated chitosan and functionalized GO, which include the following: (i) ionic crosslinking between the ammonium ion (NH_3^+) of PSC and the carboxylate ion (COO^-) of GO; (ii) temporary chelation that occurs between hydrogen atoms from the CH_2OH and CHOH of PSC, and the carboxylic group of GO;[39] and (iii) loose interaction of the ionic liquid (i.e., EMI.OTf) with the sulfonate group of PSC and with–COOH and -OH of GO. Further, a self-protonation reaction can occur by interaction of SO_3H and free NH_2 groups within the PSC membrane, resulting in the chemical cross-linking effect and higher mechanical stiffness and strength. These ionic interactions

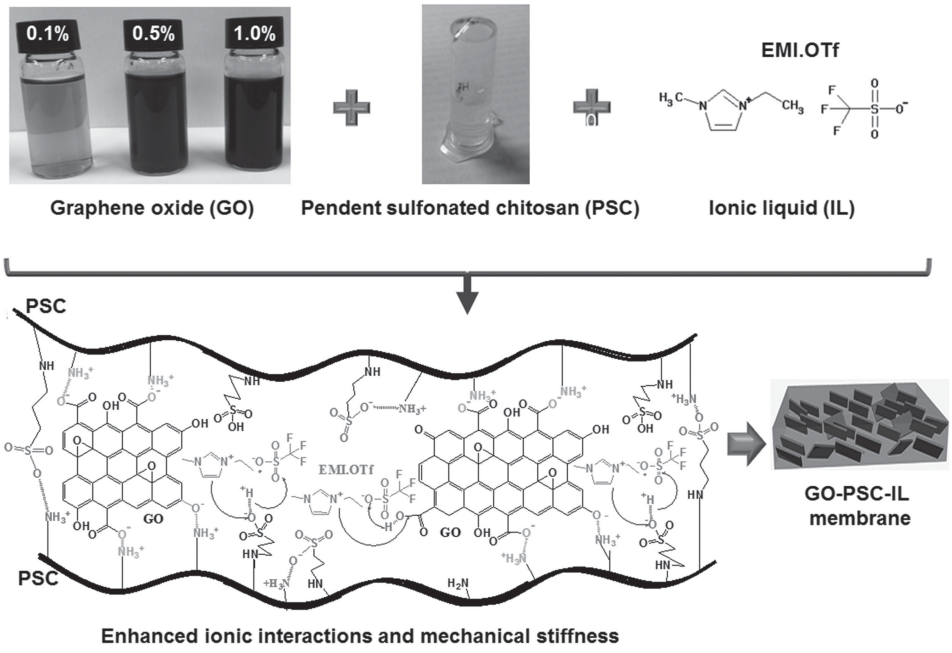

Figure 2. Synthesis of GO-PSC-IL nano-biopolymer membrane with enhanced ionic interactions and mechanical stiffness.

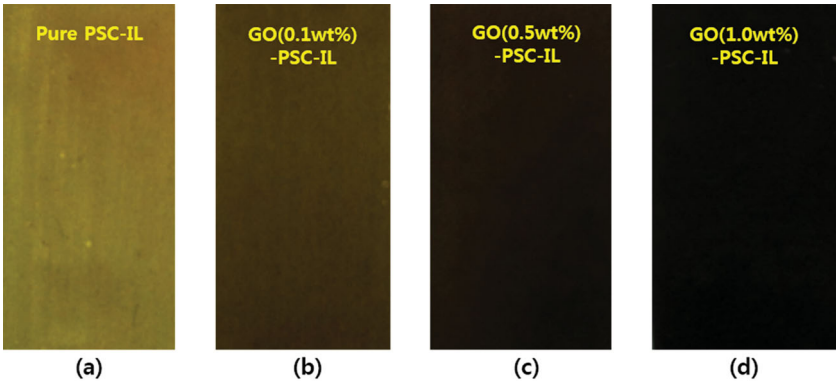

Figure 3. a–d) Photographs of GO-PSC-IL nano-biopolymer membranes.

are confirmed by FT-IR and Raman spectroscopy. **Figure 3** shows images of well-dispersed GO-PSC-IL nano-biopolymer membranes of which the color turned from yellow to black with regard to the loading level of GO in the PSC-IL matrix. This color change might be due to enhancement of the π-π conjugation in the GO network.

2.2. FT-IR

Figure 4 shows the FT-IR spectra of chitosan and sulfonated chitosan membranes. The FT-IR spectrum of PSC is in good agreement with reported PSC membranes.[37] In particular, the characteristic peaks of PSC, viz., the -OH, -SO_3H, amide I and amide II groups, appeared at 3390 cm^{-1}, 2918 cm^{-1}, 1627 cm^{-1} and 1535 cm^{-1}, respectively. Also, the peaks at 1369 cm^{-1}, 1155 cm^{-1} and 617 cm^{-1} are the stretching vibration of the SO_2 group in sulfonic acid, and these peaks indicate the presence of the SO_3H group in the PSC membrane.[40] A comparison of the FT-IR spectrum of pure chitosan with that of PSC reveals the differences between their respective absorbance bands at 1641 cm^{-1} (amide I) and 1552 cm^{-1} (amide II). The absorbance of amide II in PSC shifted from 1552 cm^{-1} to 1535 cm^{-1}, indicating that the sulfonation reaction occurred on the amine groups in the chitosan and amino groups to form secondary amide groups. Thus, the results of FT-IR analysis clearly prove the formation of the polyelectrolyte complex of the acid-base blend.

The FT-IR spectrum of GO-PSC-IL nano-biopolymer membranes was consistent with a structure composed of PSC-IL and GO, as shown in **Figure 5**. We selected GO(1.0 wt%)-PSC-IL among the GO-PSC-IL membranes for the clear comparision with qualities of the starting materials such as PSC, GO and EMI.OTf. The spectrum of GO carried peaks at 1714 cm^{-1} and 1592 cm^{-1} which correspond to C = O stretching of the carbonyl and carboxyl groups, and the -OH group appeared as a broad absorption band around 3400 cm^{-1} from the carboxy group, while the peak at 1050 cm^{-1} corresponds to O-C-O streching vibrations.[41–43] The peaks appearing at 1282 cm^{-1} and 1168 cm^{-1} correspond to SO_2 and CF_3 groups of neat EMI.OTf.[44–46]

Compared with PSC and GO, both peaks at 1535 cm^{-1} are related to NH_2 absorbance vibration, and the peak at 1714 cm^{-1} belonging to the C = O stretch of the carboxylic groups disappears in the spectra of the GO-PSC-IL membrane, and new peaks appeared at 1635 cm^{-1} and 1525 cm^{-1}. In addition, amine and hydroxyl functional groups of PSC undergo electrostatic attractions, and hydrogen bonding between PSC-IL and GO induces potentially achievable homogeneous dispersion of GO and PSC-IL in the molecular level. Good dispersion of GO enhances interfacial adhesion and increases the mechanical properties of the GO-PSC-IL nano-biopolymer membrane.

2.3. SEM

FE-SEM was employed to study surface morphologies and cross-sectional views of pure CS-IL, PSC-IL, and

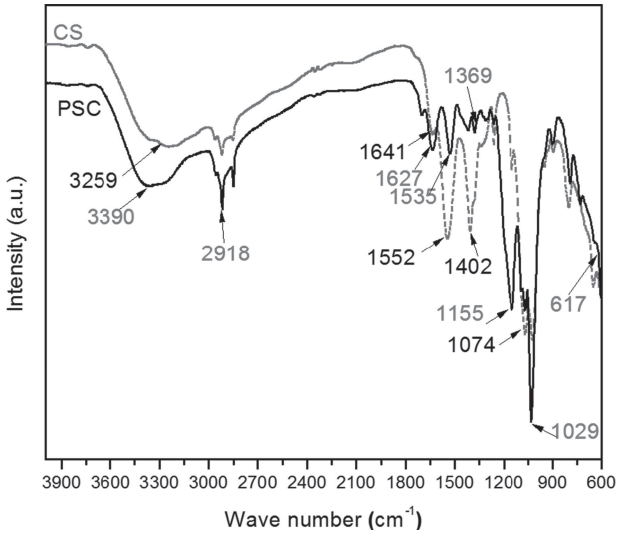

Figure 4. FT-IR spectra of pure chitosan (CS) and pendent sulfonated chitosan (PSC).

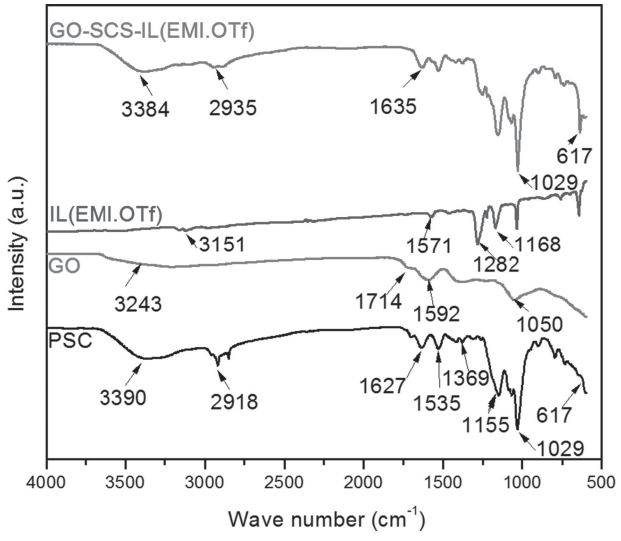

Figure 5. FT-IR spectra of PSC, GO, EMI.OTf and GO(1.0 wt%)-PSC-IL.

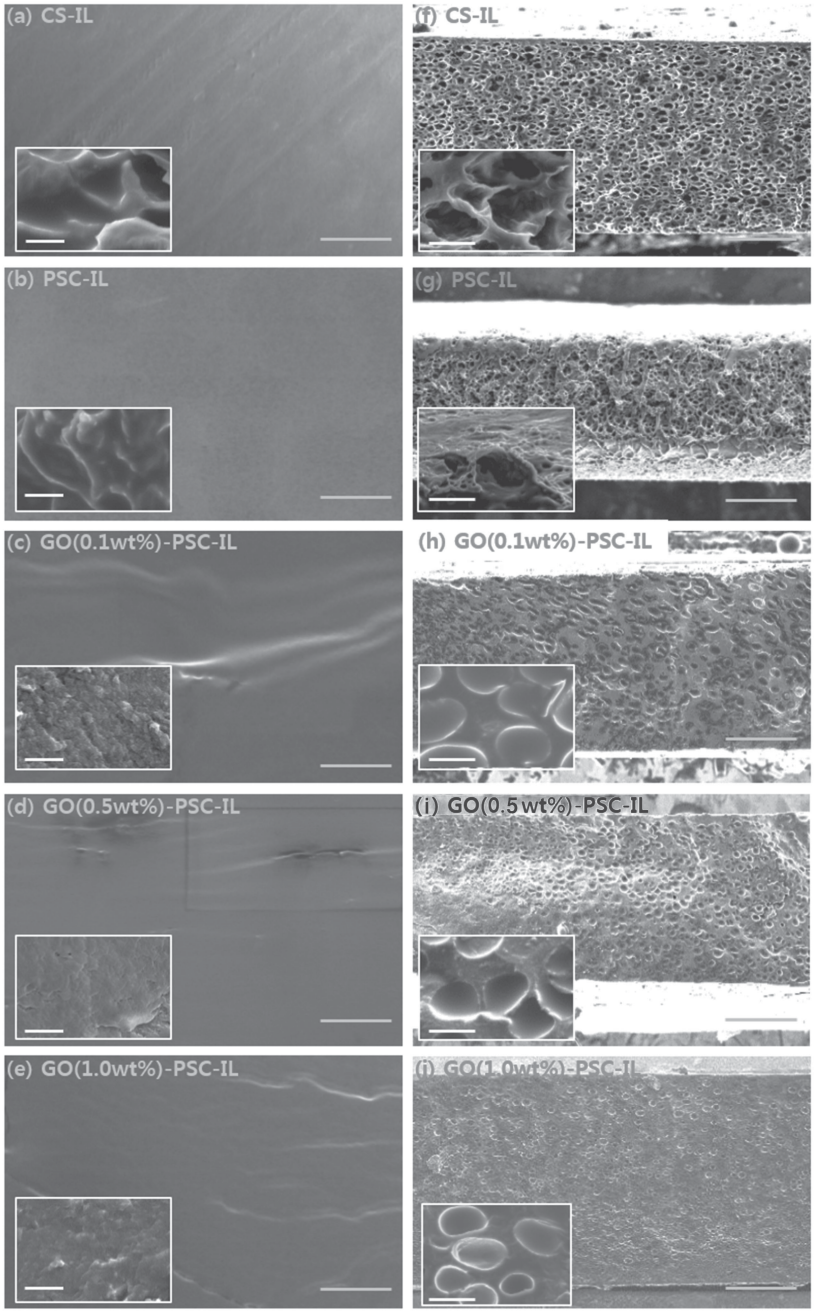

Figure 6. Representative SEM images of CS-IL, PSC-IL, GO-PSC-IL nano-biopolymer membranes; a–e) surface images and f–j) cross-sectional images after liquid nitrogen treatment with 100 μm scale bar; all inset images have 5 μm scale bars.

GO-PSC-IL membranes as shown in **Figure 6**. There is no obvious difference between the surface morphologies of the pure CS-IL and PSC-IL membranes, which both show a densely packed nature with some irregular pores in cross-sectional images in Figure 6. After the addition of GO, the GO-PSC-IL membranes showed folded surfaces with GO well dispersed in the PSC matrix without aggregation. This homogeneity of the blend membranes confirms the ionic interactions that include ionic cross-linking and hydrogen bonding between the PSC-IL and GO. However, in magnified cross-sectional images of Figures 6a–e, it might be difficult to describe the pores and ionic channels in our nano-biopolymer matrix. To clearly understand the cross-sectional morphology of the polyelectrolyte such as pore size, regularity and channel structure, the samples were fractured in a liquid nitrogen bath.[47,48] The surfaces of all chitosan-based bipolymer membranes show regular patches, and their cross-sectional images show regular pores. Interestingly, the pores are smaller in the PSC membrane than in the pure CS membrane, which indicates that a sulfonation reaction occurred on the free amine group of the PSC.

In the surface and cross-sectional images of the GO-PSC-IL nano-biopolymer with different GO loadings (0.1, 0.5, and 1.0 wt%), no phase separation was observed in the membranes, indicating that synthesized polymeric blends are well dispersed and homogeneous in nature, and also that very compact membranes are formed. The pore sizes gradually decreased due to increment of GO loadings in the PSC-IL matrix, which indicates strong protonation and improved polyelectrolyte-ionic liquid compatibiltiy.[48] The in situ one-pot polymerization technique produces a homogeneous dispersion of the GO-PSC-IL membrane in which GO maintains individual nanosheets without serious restacking phenomena.

The cross-sectional SEM images show that the GO sheets are packed tightly within the polymer matrix, further supporting good compatibility and a strong gluing property between PSC-IL and GO(Supporting Information Figure S1). Under an electrical stimulation, the EMI.OTf can be dissociated and has a mobility within the PSC-GO matrix due to temporary and weak ionic bonding between PSC and GO. Thus, the proposed novel in situ one-pot method is an effective approach to maximize the reinforcing and ionic interactions among PSC, GO and IL to produce highly performaning GO-PSC-IL artificial muscles.

2.4. XRD and Raman Spectra

X-ray diffraction (XRD) analysis of GO-PSC-IL nano-biopolymer membranes confirms that GO nanoflakes are present in the nano-biopolymer membranes and can affect the crystallinity of PSC-IL, as shown in **Figure 7**. It can be seen that there are two distinct diffraction peaks that appeared as a broad peak and a sharp peak at 2θ values of 22.3° and 12° that provided the clear evidence of the semi-crystalline nature of PSC[37] and

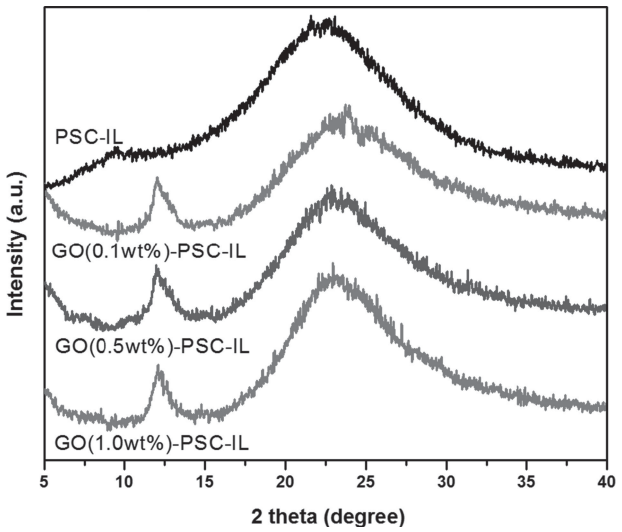

Figure 7. XRD pattern of PSC-IL, GO(0.1 wt%)-PSC-IL, GO(0.5 wt%)-PSC-IL and GO(1.0 wt%)-PSC-IL.

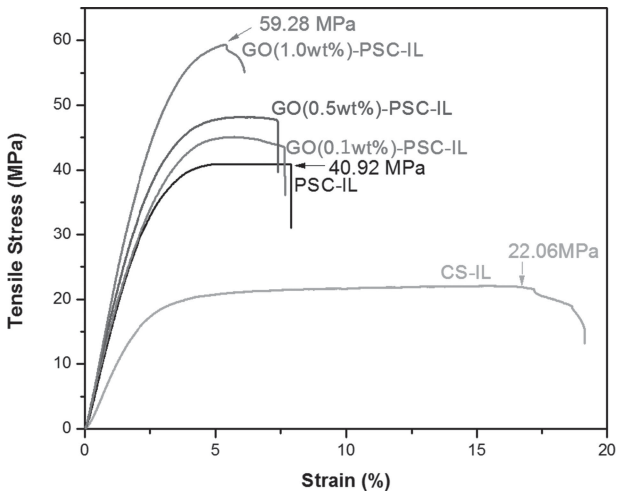

Figure 9. Stress-strain curves of CS-IL, PSC-IL and GO-PSC-IL nano-biopolymer membranes.

GO.[41] The peak shift and shape were changed by GO loading from 0.1, 0.5, and 1.0 wt% in the PSC-IL matrix. The intensity of characteristic GO-PSC-IL peaks obviously increases as GO loading increases, and that peak heights also increase. This reveals that the degree of crystallinity of chitosan increased after adding GO. Therefore, the chemical structure of the PSC in the GO-PSC-IL nano-biopolymer membranes really changes with the increasing content of GO, indicating that there were strong chemical interaction betweens PSC and GO.

The Raman spectra were obtained to characterize the electronic structure and vibrational properties of the interactions between GO and the absorbed molecules. Peaks at 1600 cm^{-1} and 1330 cm^{-1} corresponding to the D and G bands of GO[42] were observed and a stretching vibration of S-O in the PSC-IL matrix was obtained at 1037 cm^{-1} due to the PSC. The spectrum of the GO-PSC-IL nano-biopolymer in **Figure 8** shows

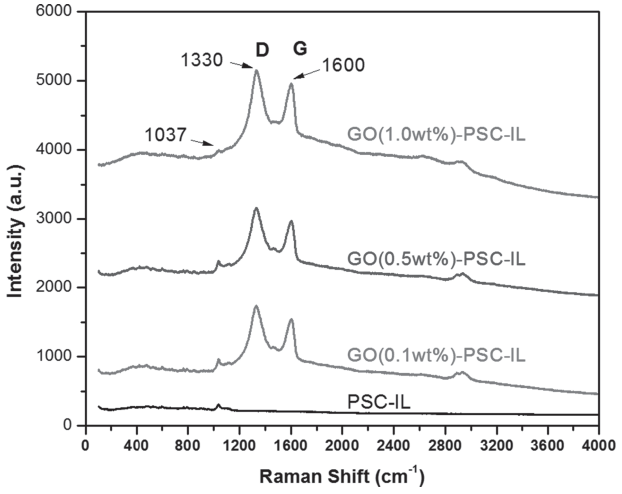

Figure 8. Raman spectra of PSC-IL, GO(0.1 wt%)-PSC-IL, GO(0.5 wt%)-PSC-IL and GO(1.0 wt%)-PSC-IL.

the typical bands of the functionalized GO in the PSC-IL matrix. However, it is noted that the intensity of characteristic GO bands increases with the increment of GO loading from 0.1 wt% to 0.5 wt% and to 1.0 wt% in the PSC-IL matrix, as shown in Figure 8. There is a change in relative intensity of the sulfonic acid band in the GO(1.0 wt%)-PSC-IL nano-biopolymer membrane, which indicates the clear difference between pure PSC-IL and GO-PSC-IL.

2.5. Tensile Test and Thermogravimetric Analysis

With the well dispersion of GO in the polymer matrix and strong interactions between the GO and the matrix, good reinforcement can be expected. To demonstrate this reinforcement, tensile tests were performed for all nano-biopolymer membranes with ionic liquid. Typical stress-strain curves are shown in **Figure 9**, and their mechanical properties are compared in **Table 1**. The results indicate that the PSC was further strengthened by the GO, and it exhibits superior mechanical stiffness and strength to those of pure chitosan and PSC membranes without GO loading. The tensile modulus of chitosan-based nano-biopolymer gradually increases through the chemical sulfonation process and with an increasing amount of GO from 0.823 GPa to 1.962 GPa. The nano-biopolymer membrane containing 1.0 wt% GO exhibits a dramatic increase of tensile modulus up to 138.4%.

The tensile strength of the nano-biopolymer membrane with 1.0 wt% of GO is 59.28 MPa, which is an increase of about 44.8% in comparison with that of PSC, and is an increase of around 168.7% over the strength of pure chitosan. Increasing the GO quantity from 0.1 to 1.0 wt%, there is a dramatic influence on the polymer tensile strength. Moreover, GO may exhibit strong interfacial interactions with the PSC to effectively restrict the movement of the polymer chain, leading to brittleness of the nano-biopolymer. Thus, the elongation at the break values of the nano-biopolymer membrane under tensile test decreased gradually as the GO content increased,

Table 1. Mechanical and chemo-electrical properties of CS-IL, PSC-IL and GO-PSC-IL nano-biopolymer membranes.

Membrane	IEC [mequiv./g]	Ionic conductivity [S/cm]	Tensile modulus [GPa]	Tensile Strength [MPa]	Elongation at break [%]
CS-IL	1.20	1.135×10^{-6}	0.823	22.06	19.14
PSC-IL	1.42	1.450×10^{-6}	1.542	40.92	7.89
GO(0.1 wt%)-PSC-IL	1.61	9.914×10^{-6}	1.614	45.19	7.63
GO(0.5 wt%)-PSC-IL	1.93	1.305×10^{-5}	1.894	48.19	7.38
GO(1.0 wt%)-PSC-IL	2.60	2.770×10^{-5}	1.962	59.28	6.11

as listed in Table 1. This consistency indicates that the well-dispersion GO particles in the PSC polymer matrix, and the strong interaction between the filler and the matrix, contributes to the emergent superior mechanical properties of the GO-PSC-IL membranes.

Figure 10 shows that TGA thermograms of PSC and PSC-GO membranes are similar to each other. They undergo three-stage decomposition; the first stage involves loss of water; the second corresponds to the decomposition of chitosan; the third stage involves the vaporization and elimination of volatile fragments. With the first stage between 50 °C and 200 °C, almost 16% loss of the initial weight occurs. The second stage follows with a further 20% weight loss just above 250 °C, which involves the pendent sulfonic acid groups of the chitosan polymer. The third stage of decomposition, which ends at around 550 °C, involves a weight loss of around 15% from the chitosan skeleton. This result is similar to those presented by Lien et al.[37] and Pereira et al.[43]

Next, we investigated the degradation of the PSC-IL and GO-PSC-IL nano-biopolymer membranes with EMI.OTf ionic liquid. The thermogram of the PSC-IL membrane differs from that of the GO-PSC-IL nano-biopolymer membranes. The heat degradation of the PSC-IL membrane occurs at three stages. At the first stage between 50 °C and 200 °C, a reduced weight loss of water molecules by 12% was recorded because ionic liquid was

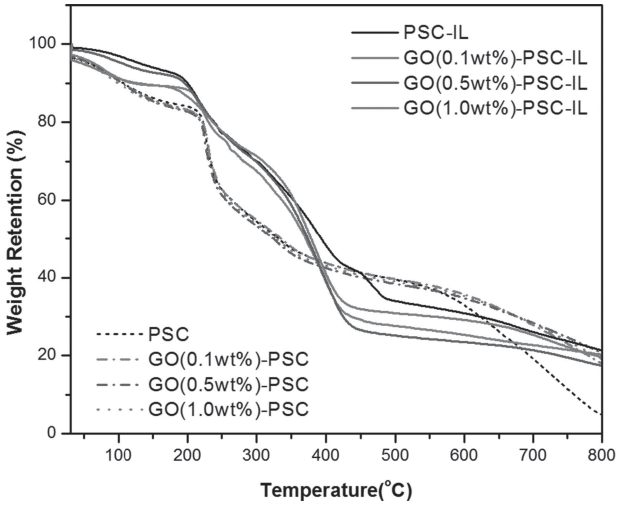

Figure 10. TGA curves of PSC, GO-PSC, PSC-IL and GO-PSC-IL nano-biopolymer membranes.

embbeded in the GO-PSC-IL mebrane. The second decomposition stage occurs from 200 °C to 300 °C and involves a weight loss of 20%, which ends with pendent sulfonic acid groups of chitosan polymer. From 300 °C to 410 °C, the third stage of decomposition involves a weight loss of 20% from the chitosan skeleton, but in the case of the PSC-IL membrane the weight loss is 15% of the chitosan skeleton. There is 5% more weight loss from the GO-PSC-IL nano-biopolymer membrane than from the PSC-IL membrane, and the GO-PSC-IL membranes are completely decomposed at 410 °C while the GO-PSC membrane is similarly degraded at 550 °C. This change might render GO-PSC-IL membranes more hydrophilic after the sulfonation process and destroy the crystalline structures. Eventually, after mixing with ionic liquid, the structure of the nano-biopolymer becames irregular, deteriorating the thermal properties.

2.6. IEC and Ionic Conductivity

Ion exchange capacity (IEC) provides an indication of the ion exchangeable groups present in a polymer matrix; these groups are responsible for the conduction of protons and are thus an indirect and reliable approximation of the ionic conductivity. Results are based on the simple calculations reported in Equation (1). The IEC values of all the membranes used in this study are listed in Table 1. The IEC values of all membranes range from 1.20 mequiv./g for CS-IL to 2.60 mequiv./g for CS(1.0 wt%)-PSC-IL, and the maximum IEC value is obtained from GO(1.0 wt%)-PSC-IL membrane. This proves that the IEC increases as GO loading increases, due to the availability of free–COOH groups of GO present within the membrane.

Next, we evaluated the ionic conductivity of the CS-IL, PSC-IL and GO-PSC-IL nano-biopolymer membranes by using Equation (2). To make high-performance ionic polymer actuators, it is very important to assess the contribution of various ionic groups in the blends. Table 1 provides ionic conductivities of CS-IL, PSC-IL, and GO-PSC-IL membranes at room temperature. The GO-PSC-IL polyelectrolyte blends exhibit higher conductivities compared to the CS-IL and PSC-IL membranes due to the interaction of SO_3H and COOH groups with EMI.OTf. The GO(1.0 wt%)-PSC-IL showed a conductivity value of 2.770×10^{-5} S/cm much higher than that of the PSC-IL membrane (1.450×10^{-6} S/cm). The high ionic conductivity can be attributed to the SO_3H, COOH, and NH_2 groups, and these ionophilic regions formed around the

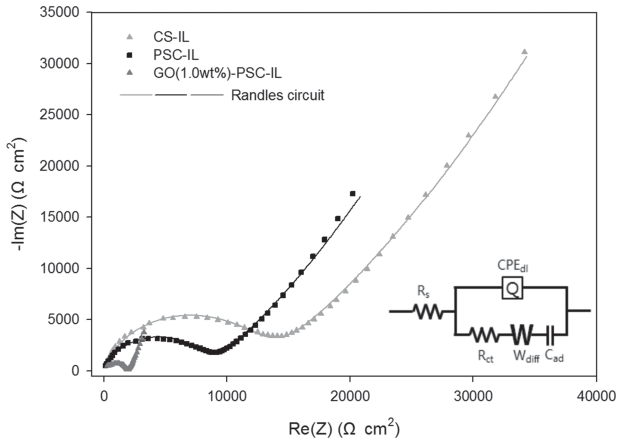

Figure 11. Nyquist plots of the CS-IL, PSC-IL, and GO-PSC-IL membranes; Inset figure shows the equivalent Randles circuit model for fitting the EIS.

cluster of side chains lead to absorption of ionic liquid, enabling easy ion transfer.[49]

2.7. EIS Analyses of the CS-IL, PSC-IL and GO-PSC-IL Membranes

The electrochemical impedance spectroscopy (EIS) can be used to confirm the electrochemical reaction among ionic liquid and functional group of GO-PSC matrix. Basically, EAP actuators based on ionic liquids can be expressed by an equivalent circuit with parallel combination of a resistor and a capacitor. Especially, in order to more accurately evaluate ionic diffusion responses of ionic type EAP actuators in the low frequency range, Warburg diffusion element and constant phase element (CPE) can be used. So, in this study the equivalent Randles circuit with Warburg diffusion element and CPE was used to model the electrochemical impdeance, as represented in **Figure 11**. The equivalent Randles circuit includes the ohmic resistance (R_s) corresponding to the summation of the electric contact resistance and the electrolyte bulk resistance in the high-frequency region, double-layer capacitance (CPE_{dl}), charge transfer resistance (R_{ct}), and Warburg diffusion elelement (W_{diff}) and adsorption capacitance (C_{ad}) in the low-frequency region.[50,51] The extrapolation of a semi-circle to the X-axis gives the ionic resistance. The ionic resistances of PSC and GO-reinforced PSC membranes were decreased because of higher ionic interaction between ionic liquid and functional groups of PSC and GO. It also reveals higher compatiblity of ionic liquid and polyelectrolyte as confirmed in cross-sectional SEM images. Also, polyelectrolyte membranes exhibit capacitive behavior as well as ionic behavior because of ionic liquid uptake, and ionic interactions among PSC, GO, and ionic liquid. Therefore, double-layer capacitance and adsorption capacitance were slightly increased. These synergistic improvements of electrochemical properties can greatly increase the bending performance of the GO-PSC-IL nano-biopolymer actuator. These fitting parameters of impedance spectroscopy are shown in **Table 2**.

Table 2. Parameter values obtained by fitting the impedance data of the CS-IL, PSC-IL and GO-PSC-IL membranes.

Membranes	R_s [Ω·cm²]	CPE_{dl} [S·s^n/cm²]	n	R_{ct} [Ω·cm²]	W_{diff} [S·s$^{0.5}$/cm²]	C_{ad} [μF/cm²]
CS-IL	116.61	3.163×10^{-9}	0.8564	12970	4.128×10^{-6}	1.744
PSC-IL	130.68	4.488×10^{-9}	0.8319	8368	7.111×10^{-6}	3.538
GO(1.0 wt%)-PSC-IL	270.67	4.554×10^{-9}	0.8235	1877	7.303×10^{-5}	6.168

2.8 Harmonic Responses of the GO-PSC-IL Actuator

In the following chapers, we analyzed the actuation performances of the prepared artificial muscles. **Figure 12**a shows the harmonic motion of the PSC-IL, GO(0.1 wt%)-PSC-IL, GO(0.5 wt%)-PSC-IL and GO(1.0 wt%)-PSC-IL nano-biopolymer actuators under an applied voltage of AC 2V with an excitation frequency of 0.1 Hz. The bending curvature of an actuator is given by equation 3. The maximum bending curvature of the GO-PSC-IL actuator, which had the highest weight ratio of 1.0 wt% GO, was up to 5.03 m^{-1}, which was 1.8 times

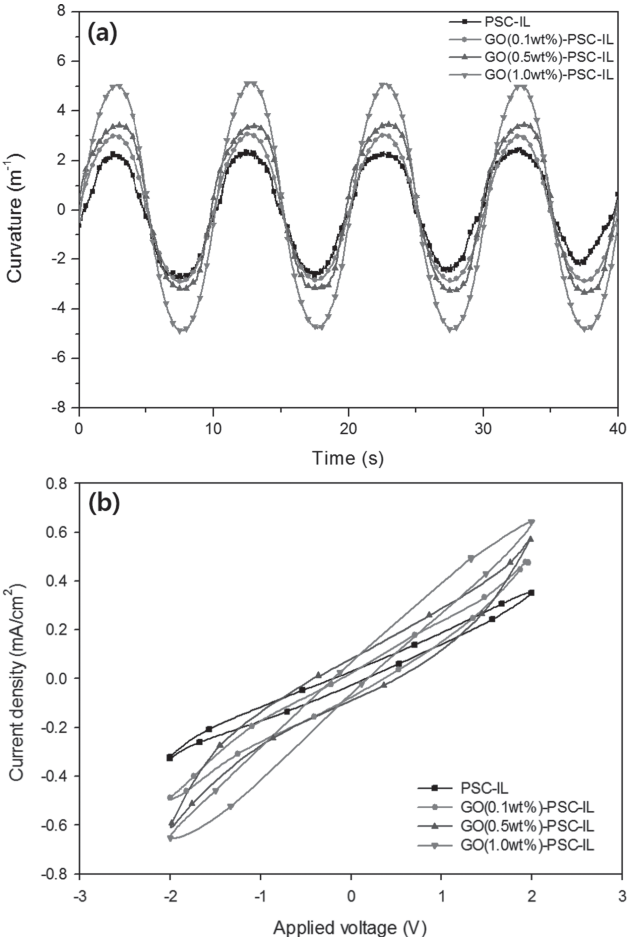

Figure 12. Harmonic responses of PSC-IL and GO-PSC-IL actuators under sinusoidal electrical input, $V(t) = 2V\sin(2\pi \cdot 0.1 \cdot t)$: a) time history of curvature and b) current-voltage diagram.

more than pure PSC-IL, which itself had a bending curvature of 2.67 m^{-1}. The peak bending curvatures were 3.42 m^{-1} for GO(0.5wt%)-PSC-IL and 2.96 m^{-1} for GO(0.1wt%)-PSC-IL. Therefore, the harmonic response of the GO-PSC-IL nanobiopolymer actuators was improved significantly as the GO loading quantity increased. These observations indicate that the high ionic conductivity, improved electrochemical capacitance of GO-PSC-IL matrix, high mechanical properties and strong ionic interactions among PSC, GO and IL had a considerable influence on much higher bending peformance of the GO(1.0 wt%)-PSC-IL actuator. Much larger bending deformation of GO(1.0 wt%)-PSC-IL actuator will produce much higher kinetic energy, but also will require much higher external work done by the electrical input. This tendency is observed in the current-voltage responses as shown in Figure 12b. The circle area, which means a dissipated specific input energy, increases with respect to the increasing content of graphene oxide in the polymer matrix, and the GO(1.0 wt%)-PSC-IL has the maximum value of the current density upto 0.643 mA/cm^2 due to much larger bending deformation.

Next, we investigated the actuation performance of the GO(1.0 wt%)-PSC-IL actuator according to peak voltage changes of sinusoidal electric inputs with the same excitation frequency of 0.1 Hz as shown in **Figure 13**a. As the peak voltage increases, the bending curvature of the GO-PSC-IL actuator monotonically increases without a large distortion due to relativley higher ionic interaction and large capacitance in the ionic pores homogeneously distrubuted in the GO-PSC-IL matrix. The peak bending curvature of the GO(1.0 wt%)-PSC-IL actuator reached up to 13.16 m^{-1} from an applied voltage of 10 V, 7.46 m^{-1} from 5 V, and 5.0 m^{-1} from 2 V. To consider the current-voltage response of GO(1.0 wt%)-PSC-IL actuator according to driving voltages, current-voltage diagrams were drawn as shown Figure 13b. The circle area, which corresponds to the dissipated electrical input energy, increases with the increasing driving voltages.

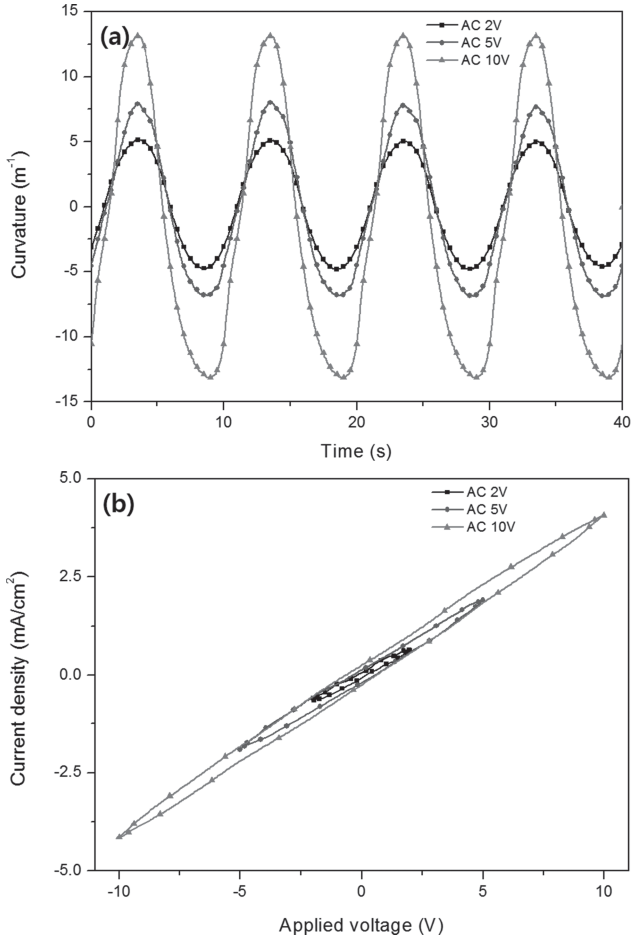

Figure 13. Harmonic responses of GO(1.0 wt%)-PSC-IL actuator at sinusoidal excitation of different driving voltages: a) time history of curvature and b) current–voltage diagram.

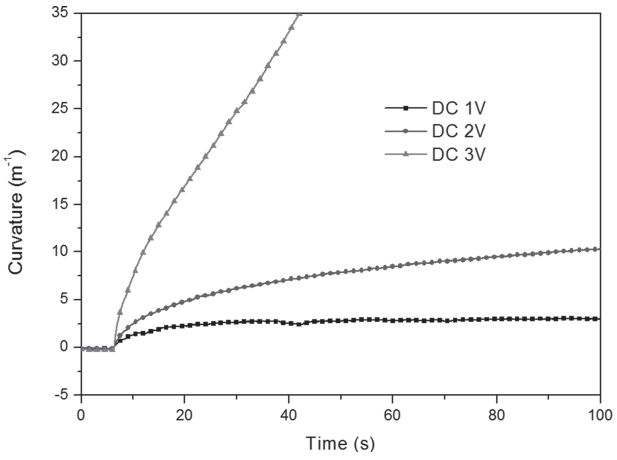

Figure 14. Step responses of GO(1.0 wt%)-PSC-IL actuator according to driving voltages.

Figure 14 shows the step responses of the GO(1.0 wt%)-PSC-IL actuator under different electrical inputs. As the excitation voltage increases, the actuation performance also increases without the back-relaxation phenomenon, which is one of the main drawbacks of conventional ionic polymer-metal composite actuators. This improvement can be attributed to the higher ionic conductivity and larger capacitance, and effective blocking or delay of ionic liquid migration in the reduced ionic pores or channels of GO(1.0 wt%)-PSC-IL under lower applied voltages. Surprisingly, the curvature of the actuator under the 3 V step input dramatically increases as much higher as we can not measure tip displacement with laser displacement sensors. It was expected when we measured several superior electro-chemo-mechanical material properties and observed the reduced pore sizes in the morphological images. Also, it reveals that the actuation force generated by ionic liquid migration in the GO-PSC-IL actuator can overcome the restoring force by mechanical stiffness of the cantilever beam at a relatively higher voltage.

Figure 15 shows the deformed shapes of the GO(1.0 wt%)-PSC-IL actuator under DC 5.0 V as time goes. The actuator did not show the back-relaxation phenomenon. The tip displacement of the as-fabricated actuator exceeded the range of the employed laser displacement sensor within 5 s, and it continued to deform with a constant curvature at very rapid speed in the following 15 s interval. The fast response and large deformation

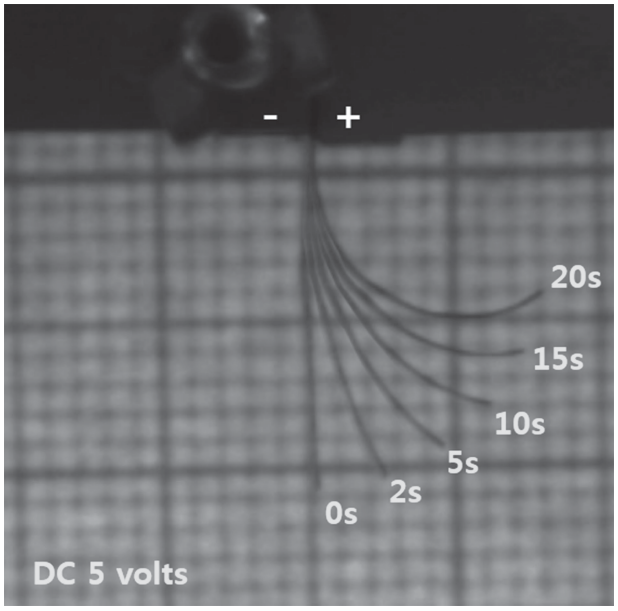

Figure 15. Electro-mechanically deformed shapes of GO-PSC-IL actuator under a step input with DC 5 Volts ($V(t) = 5\ V \cdot u(t)$).

of the GO(1.0 wt%)-PSC-IL actuator at the higher DC excitation were exhibited. Also, the deformation increased steadily as long as the voltage was applied quasi-statically due to effective ionic liquid migration in the homogeneous ionic pores.

3. Conclusions

In summary, we report a novel high-performance electro-active nano-biopolymer based on pendent sulfonated chitosan (PSC), functionalized graphene oxide (GO) and ionic liquid (IL) with superior electro-chemo-mechanical properties. The pendent sulfonated chitosan and functionalized graphene oxide show strong interfacial ionic interactions at the molecular level between amine and carboxylic acid groups, resulting in the formation of chemically stable nano-biopolymer membranes with high mechanical strength and stiffness. The GO(1.0 wt%)-PSC-IL nano-biopolymer membrane exhibits a tensile strength increased up to 44.8% and a tensile modulus increased by over 27.2% as compared to the pure chitosan membrane. In addition, enhanced protonation and uptake of ionic liquid in the GO-PSC-IL membrane, coming from the ionic interaction with the sulfonic acid of the PSC as well as the carboxylic and hydroxy groups in GO, result in two times higher ionic exchangeble capacity and eighteen times higher ionic conductivity. These synergistic effects are beneficial in making a high-performance nano-biopolymer actuator which shows enhanced bending deformation under harmonic and step inputs as compared to the pristine chitosan actuator, and the GO-PSC-IL actuators did not show the back-relaxation phenomenon. Moreover, all used materials are naturally abundant, economically cheap and eco-friendly, so these GO-PSC-IL actuators can be a promising candidate for energy-efficient artificial muscles, biomimetic robots and disposable biomedical devices in the future.

4. Experimental Section

Chitosan was purchased from the Aldrich Chemical Co., USA. The degree of deacetylation was around 80% and molecular weight was about 400 000 Da. Acetic acid, 1,3-propane sultone, potassium permanganate ($KMnO_4$), sodium nitrate ($NaNO_3$), sulfuric acid (H_2SO_4), hydrogen peroxide (H_2O_2), and 1-ethyl-3-methylimidazolium trifluoromethane sulfonate (EMI.OTf, ≥ 98.0%) were obtained from Aldrich and used as received. High purity natural graphite (purity of 99%, average size of 200 μm) was purchased from Infrazone, Korea.

Preparation of Sulfonated Chitosan:[37] 1.0 g of chitosan was dissolved in 80 mL of 2 wt% aqueous acetic acid solution. After stirring for 1 h, 1,3-propane sultone (0.4 g) was added and the mixture was allowed to react at 60 °C for 6 h. The resultant solution was poured into acetone to precipitate. The precipitated product was washed sufficiently with acetone and methanol sequentially, and dried in a thermostat oven at 50 °C for one day. The obtained product was the pendent sulfonated chitosan (PSC). The degree of sulfonation refers to the degree of substitution of alkyl sulfonic groups for amino groups in the chitosan. The molar ratio of the propane sultone unit that reacted with the glucosamine unit was 0.5, as shown in Figure 1.

Preparation of Few Layered Graphene Oxide:[38] Graphene oxide was prepared from natural graphite by the well-known Hummers method with little modification. In brief, 2 g of natural graphite powder was added into a 250 mL beaker, and then 1 g of $NaNO_3$ and 46 mL of H_2SO_4 were added into it sequentially while stirring in an ice-bath. Next, 6 g of $KMnO_4$ was added slowly into the beaker while stirring and the temperature was maintained below 20 °C. The ice-bath was removed after 5 min and the reaction mixture was heated at 35 °C for 30 min, and then 92 mL of water was added slowly to the reaction mixture. The mixture was then stirred for another 15 min. Next, 80 mL of hot water at 60 °C and a 30% H_2O_2 aqueous solution were added to reduce the residual $KMnO_4$ until no bubbles were present. Finally, the reaction mixture was centrifuged at 8000 rpm for 30 min, and the obtained powder was washed by warm water until the pH reached ≈7. The obtained yellow-brown powder was re-dispersed into ultrapure water and treated with mild ultrasound for 30 min, and homogeneous suspensions with different concentrations were formed after filtering the trace black residues. Graphene oxide powder was obtained after drying the suspension at 60 °C.

Preparation of GO-PSC-IL Membranes: GO-PSC-IL nano-biopolymer membranes were prepared using a solution mixing process. After synthesis of PSC solution as previously described in Section 3.1, the aqueous GOs (1 mg, 5 mg and 10 mg in 50 mL of DI water) were subsequently mixed with the PSC solution and stirred for 2 h. Next, 0.5 g of EMI.OTf (IL) was added to the reaction mixtures separately and stirred for 1h at room temperature. Before casting on the glass plates, the polymer solutions were degassed by applying a vacuum to eliminate the air bubbles. Next, the GO-PSC-IL polyelectrolyte solutions were cast on glass plates and evaporated at 60 °C for 24 h to obtain membranes with a thickness of about 0.3 mm. A series of GO-PSC-IL nano-biopolymer membranes were designated as GO(0.1 wt%)-PSC-IL, GO(0.5 wt%)-PSC-IL and GO(1.0 wt%)-PSC-IL as listed in Table 1. It was difficult to prepare the film with more than 1.0 wt% of graphene oxide due to formation of a highly viscous solution and the occurance of phase separation, resulting in inferior mechanical properties such as extreme brittleness.

FTIR, SEM, XRD, and Raman Spectroscopy: The FT-IR spectra of the CS, PSC and GO-PSC-IL nano-biopolymer membranes were scanned using an IFS66V/S & HYPERION 3000, Bruker Optiks (Germany), and these spectra are shown in Figures 4 and 5. Scanning electron microscope (SEM) observations were carried out on an FEI Sirion FESEM, 30 kV microscope. The films were thoroughly dried before capturing the images, and the surface morphology and cross sectional images were studied. The SEM images for the CS, PSC and GO-PSC-IL membranes are shown in Figure 6. X-ray diffraction (XRD) of the nano-biopolymers was measured using a DMAX-Ultima III X-ray diffractometer in the range of 5 to 40 (Figure 7). Raman spectra were recorded on an FT-Raman from Bruker Optics (Germany) with a 1064 nm Laser

spectrophotometer, a spectral range of 4000–100 cm^{-1} and a resolution of 1 cm^{-1} (Figure 8).

Tensile-Stress Curves and Thermogravimetric Analysis: The tensile strength, modulus properties and elongation of the GO-PSC-IL nano-biopolymer membranes were determined using a table-top universal testing machine (AGS-X+250, Shimadzu Corp., Japan.) equipped with a 1 kN load cell. The test speed was set to a rate of 10 mm/min. The cross-sectional area of the membrane samples was measured before testing with a micrometer. The gauge length between the grips was 10 mm. All tested samples had a regular rectangular shape. TGA measurements of the CS, PSC and GO-PSC-IL nano-biopolymer membranes were done on a Thermogravimetric Analyzer (TG209F3) from NETZSCH (Germany), over temperatures ranging between 40 and 800 °C under a Nitrogen atmosphere condition and at a heating rate of 10 °C/min. All membranes were air dried.

Electrochemical Properties: Ion Exchange Capacity, Ionic Conductivity, and EIS Analysis: Ion exchange capacity (IEC) indicates the number of milliequivalents of ions in 1 g of the dry GO-PSC nano-biopolymer. To determine the ion exchange capacity, the titration method was applied, using Phenolphthalein as an indicator. The acidic form of the membrane was converted to the sodium form by immersion in 1 M NaCl solutions for 24 h. The exchanged ions in the solution were titrated with a 0.1 M NaOH solution. The IEC values were determined by the following equation:

$$IEC = \frac{\text{Consumed NaOH(mL)} \times \text{molarity of NaOH}}{\text{Weight of the membrane}} \quad (1)$$

The ionic conductivities of the ionic liquid doped nano-biopolymer membranes were calculated through the electrochemical impedance spectroscopy data obtained from a complex impedence analyzer (VersaSTAT 3 potentiostat/galvanostat, Princeton Applied Research) over a frequency range of 10–1 MHz under a maximum voltage of 0.1 V. Membranes of a circular shape with a 6 mm diameter and an ECC-STD electrochemical cell (EL-CELL) with two stainless steel electrodes were used. The ionic conductivity can be calculated with the following equation:

$$\text{Ionic conductivity} = \frac{1}{R(\Omega)} \times \frac{L(\text{cm})}{S(\text{cm}^2)} [\text{S/cm}] \quad (2)$$

where R is the ionic resistance, i.e., charge transfer resistance, which is calculated from the intercept of the semicircle at the low-frequency side of the Nyquist plot with the real axis, and L and S are the thickness and area of the membranes. The data obtained by electrochemical impedance spectroscopy was fitted by using ZSimpWin 3.21 software.

Fabrication of Actuator and Setup for Actuation Tests: Thin gold electrodes were deposited on both sides of the as-received GO-PSC-IL membranes using a Au coater. The size of the actuator was 4 mm × 20 mm × 0.3 mm. The actuator was clamped with about a 4 mm × 5 mm area at one end. The experimental setup for the measurement of actuation consisted of a PXI 6252 data acquistion board, a current amplifier (UPM1503, Quanser), a charged-couple device camera (XC-HR50, Sony) and a laser displacement sensor (LK-031, Keyence). All the data were acquired and controlled by an NI-PXI system(1042Q, NI) by using the LabVIEW program.

The bending curvature κ generated in the actuator was estimated by the following equations.

$$\kappa = \frac{1}{R} = 2\delta / (l^2 + \delta^2) \quad (3)$$

where R, δ, and l are the radius of curvature, the tip displacement and the free length of the actuator.

Supporting Information

Supporting Information is available from the Wiley Online Library or from the author.

Acknowledgements

J.H.J. and R.K.C. contributed equally to this work. This work was supported by a National Research Foundation of Korea Grant funded by the Korean Government (No. R0A-2008-000-20012-0) and (2012R1A2A2A0104754). This work was supported by Midcareer Researcher Program through a NRF grant funded by the MEST (2012-0383).

Received: December 1, 2012
Revised: March 25, 2013
Published online: June 28, 2013

[1] Y. Osada, H. Okuzaki, H. Hori, *Nature* **1992**, *355*, 242.
[2] T. F. Otero, E. Angulo, J. Rodriguez, C. Santamaria, *J. Electroanal. Chem.* **1992**, *341*, 369.
[3] Q. Pei, O. Inganas, *Adv. Mater.* **1992**, *4*, 227.
[4] K. Oguro, Y. Kawami, H. Takenaka, *U.S. Patent No. 5268082*, **1993**.
[5] M. Shahinpoor, K. J. Kim, *Smart Mater. Struct.* **2001**, *10*, 819.
[6] J. Lu, S.-G. Kim, S. Lee, I. K. Oh, *Adv. Funct. Mater.* **2008**, *18*, 290.
[7] R. H. Baughman, C. Cui, A. A. Zakhidov, Z. Iqbal, J. N. Barisci, G. M. Spinks, G. G. Wallace, A. Mazzoldi, D. De Rossi, A. G. Rinzler, O. Jaschinski, S. Roth, M. Kertesz, *Science* **1999**, *284*, 1340.
[8] K. Mukai, K. Asaka, T. Sugino, K. Kiyohara, I. Takeuchi, N. Tersawa, D. N. Futaba, K. Hata, T. Fukushima, T. Aida, *Adv. Mater.* **2009**, *21*, 1582.
[9] S. Park, J. An, J. W. Suk, R. S. Ruoff, *Small* **2010**, *6*, 210.
[10] J. H. Jung, J. H. Jeon, V. Sridhar, I. K. Oh, *Carbon* **2011**, *49*, 1279.
[11] L. Lu, J. Liu, Y. Hu, Y. Zhang, H. Randriamahazaka, W. Chen, *Adv. Mater.* **2012**, *24*, 4317.
[12] R. Pelrine, R. Kornbluh, Q. Pei, J. Joseph, *Science* **2000**, *287*, 836.
[13] Q. M. Zhang, H. Li, M. Poh, F. Xia, Z. Y. Cheng, H. Xu, C. Huang, *Nature* **2002**, *419*, 284.
[14] K. Fukuda, T. Sekitani, U. Zschieschang, H. Klauk, K. Kuribara, T. Yokota, T. Sugino, K. Asaka, M. Ikeda, H. Kuwabara, T. Yamamoto, K. Takimiya, T. Fukushima, T. Aida, M. Takamiya, T. Sakurai, T. Someya, *Adv. Funct. Mater.* **2011**, *21*, 4019.
[15] M. Y. Ozsecen, M. Sivak, C. Mavroidis, *Proc. SPIE* **2010**, *7647*, 764737.
[16] S. W. Yeom, I.K. Oh, *Smart Mater. Struct.* **2009**, *18*, 085002.
[17] F. Carpi, D. D. Rossi, *IEEE T. Info. Technol. Biomed.* **2005**, *9*, 295-318.
[18] K. Ren, S. Liu, M. Lin, Y. Wang, Q. M. Zhang, *Sens. Actuators, A* **2008**, *143*, 335.
[19] E. Smela, *Adv. Mater.* **2003**, *15*, 481.
[20] T. F. Otero, J. J. Sanchez, J. G. Martinez, *J. Phys. Chem. B* **2012**, *116*, 5279.
[21] M. J. Han, J. H. Park, J. Y. Lee, J. Y. Jho, *Macromol. Rapid Commun.* **2006**, *27*, 219.
[22] J. H. Jeon, S. P. Kang, S. Lee, I. K. Oh, *Sens. Actuators, B* **2009**, *143*, 357.
[23] X. L. Wang, I. K. Oh, L. Xu, *Sens. Actuators, B* **2010**, *145*, 635.
[24] X. L. Wang, I. K. Oh, S. Lee, *Sens. Actuators, B* **2010**, *150*, 57.
[25] M. Rajagopalan, I. K. Oh, *ACS Nano* **2011**, *5*, 2248.
[26] J. Kim, S. Yun, Z. Ounaies, *Macromolecules* **2006**, *39*, 4202.
[27] J. Li, V. Sridhar, C. D. Kee, I. K. Oh, *Biomacromolecules*, **2011**, *12*, 2048.
[28] J. H. Jeon, I. K. Oh, C. D. Kee, S. J. Kim, *Sens. Actuators, B* **2010**, *146*, 307.
[29] N. Wang, Y. Chen, J. Kim, *Macromol. Mater. Eng.* **2007**, *292*, 748.
[30] L. Lu, W. Chen, *Adv. Mater.* **2010**, *22*, 3745.
[31] J. Li, W. Ma, L. Song, Z. Niu, L. Cai, Q. Zeng, X. Zhang, H. Dong, D. Zhao, W. Zhou, S. Xie, *Nano Lett.* **2011**, *11*, 4636.

[32] X. L. Wang, I. K. Oh, J. B. Kim, *Compos. Sci. Technol.* **2009**, *69*, 2098.
[33] J. H. Jung, S. Vadahanambi, I. K. Oh, *Compos. Sci. Technol.* **2010**, *70*, 584.
[34] I. K. Oh, J. H. Jung, J. H. Jeon, S. Vadhanambi, *Smart Mater. Struct.* **2010**, *19*, 0750009.
[35] W. Sun, Y. Wang, X. Li, J. Wu, T. Zhan, K. Jiao, *Electroanal.* **2009**, *21*, 2454.
[36] A. Pinker, K. N. Marsh, S. Pang, M. P. Staiger, *Chem. Rev.* **2009**, *109*, 6712.
[37] H. S. Tsai, Y. Z. Wang, J. J. Lin, W. F. Lien, *J. Appl. Polym. Sci.* **2010**, *116*, 1686.
[38] S. Park, R. S. Ruoff, *Nat. Nanotechnol.* **2009**, *4*, 217.
[39] B. Smitha, S. Sridhar, A. A. Khan, *Macromolecules* **2004**, *37*, 2233.
[40] C. N. R. Rao, *Chemical applications of infrared spectroscopy*, Academic Press, New York **1963**.
[41] V. K. Rana, M. C. Choi, J. Y. Kong, G. Y. Kim, M. J. Kim, S. H. Kim, S. Mishra, R. P. Singh, C. S. Ha, *Macromol. Mater. Eng.* **2011**, *296*, 131.
[42] M. A. Pimenta, G. Dresselhaus, M. S. Dresselhaus, L. A. Cancado, A. Jorio, R. Sato, *Phys. Chem. Chem. Phys.* **2007**, *9*, 1276.
[43] C. G. T. Neto, J. A. Giacometti, A. E. Job, F. C. Ferreira, J. L. C. Fonseca, M. R. Pereira, *Carbohydr. Polym.* **2005**, *62*, 97.
[44] J. F. Huang, G. A. Baker, H. Luo, K. Hong, Q. F. Li, N. J. Bjerrum, S. Dai, *Green Chem.* **2006**, *8*, 599.
[45] G. H. Lane, P. M. Bayley, B. R. Clare, A. S. Best, D. R. MacFarlane, M. Forsyth, A. F. Hollenkamp, *J. Phys. Chem. C* **2010**, *114*, 21775.
[46] L. Zhai, Q. Zhong, C. He, J. Wang, *J. Hazard. Mater.* **2010**, *177*, 807.
[47] A. Salam, R.A. Venditti, J.J. Pawlak, K. EI-Tahlawy, *Carbohydr. Polym.* **2011**, *84*, 1221.
[48] J. Schaure, A. Sikora, M. Pliskova, J. Malis, P. Mazur, M. Paidar, K. Bouzek, *J. Membr. Sci.* **2011**, *367*, 332.
[49] K. Miyatake, K. Oyaizu, E. Tsuchida, A. S. Hay, *Macromolecules* **2001**, *34*, 2065.
[50] T. Pajkossy, T. Wandlowski, D. M. Kolb, *J. Electroanal. Chem.* **1996**, *414*, 209.
[51] A. Janes, L. Permann, M. Arulepp, E. Lust, *J. Electroanal. Chem.* **2004**, *569*, 257.